Journal of
Applied Crystallography
ISSN 0021-8898

Received 16 August 2006
Accepted 1 February 2007

Polarized small-angle neutron scattering study of two-dimensional spatially ordered systems of nickel nanowires

N. A. Grigoryeva,[a]* S. V. Grigoriev,[b] H. Eckerlebe,[c] A. A. Eliseev,[d] A. V. Lukashin[d] and K. S. Napolskii[d]

[a]Physical Faculty, St Petersburg State University, St Petersburg, 198504, Russia, [b]Petersburg Nuclear Physics Institute, Gatchina, St Petersburg, 188300, Russia, [c]GKSS Forschungszentrum, Geesthacht, 21502, Germany, and [d]Higher School of Materials Science, Moscow State University, Moscow, 119899, Russia.
Correspondence e-mail: phylipp@gtn.ru

The magnetic and structural properties of two-dimensional spatially ordered systems of ferromagnetic nickel nanowires embedded into an Al_2O_3 matrix have been studied using polarized small-angle neutron scattering (polarized SANS). We measured the total (nuclear and magnetic) scattering $I(q)$ as a polarization-independent scattering, the field-dependent scattering as $I_{\mathbf{H}}(q) = \mathrm{I}(q, \mathbf{H}) - I(q, 0)$, where $\mathbf{H}$ is the magnetic field, and the nuclear-magnetic interference as a polarization-dependent (P) scattering $\Delta I(q, P)$. A typical scattering pattern is composed of the diffuse small-angle scattering and the Bragg peak. It is shown that the introduction of Ni into the matrix does not change the position of the Bragg peak but results in an increase of the scattering intensity both in the small-angle region and at the Bragg positions. An external magnetic field was applied perpendicular or parallel to the long dimension of the nanowires in order to reveal the anisotropic properties of the magnetic system. It is shown that, firstly, the magnetic-field-dependent scattering $I_{\mathbf{H}}(q)$ provides new and principally different information as compared with the interference term $\Delta I(q)$. Secondly, two contributions to the interference term $\Delta I(q)$ (ascribed to the diffuse scattering and to the diffraction peaks) have different signs indicating different origins of the scattering objects. Thirdly, polarized SANS gives a detailed picture of the magnetization process, which could not be obtained by methods of standard magnetometry.

1. Introduction

Nanomaterials have attracted great attention in the last decade because of their numerous applications in industry. Today, advanced technologies require preparation of nanosystems with specified size and morphology of particles. For another ten years at least, the main branch of the information carriers industry will rely upon magnetic information storage. From a technological point of view, the special role in creation of the components for magnetic information storage belongs to high-quality nanostructures and nanocomposites with detached, strongly anisotropic and regularly ordered magnetic nanoparticles. Aluminium oxide is considered to be a potential matrix for the preparation of magnetic nanocomposites and as a promising candidate for data storage devices. It has been estimated that a bit density several times greater than that currently possible could be achieved from this type of composite material. Here, not only the size control of individual nanoparticles is important, but also their mutual disposition in the mesostructure formed by the alumina template as well as their structural anisotropy provoking the magnetic anisotropy of the metal nanoparticles in the pores.

Several authors have reported the investigation of self-organization of mesopore channels formed during the anodization process, however, most of them involve only electron microscopy or scanning probe microscopy studies (Jessensky *et al.*, 1998; Nielsch *et al.*, 2002; Li *et al.*, 1998; Masuda *et al.*, 1997), which are known for their locality and only a few studies rely upon a small-angle scattering technique for quantitative characterization. Although SANS and small-angle X-ray scattering (SAXS) methods have been extensively used for studying spatially ordered materials, few studies have been done on the characterization of anodic aluminium oxide (AAO) membranes and AAO-based nanocomposites. At the same time these methods can provide extremely valuable information on pore structure (interpore distance, diameter and length) and organization (spatially correlated volumes, AAO domain size). Recently SAXS was successfully applied for the calculation of periodicity parameters of anodic alumina films and the determination of the loading value and homogeneity of cobalt wires grown in AAO templates (Benfield *et al.*, 2004). However, the penetration distance of both electron and X-ray irradiation to solid state objects usually equals a few micrometres only, while characterization of alumina membranes (with thickness sometimes exceeding several hundred micrometres) requires higher penetration depths, which could be achieved using neutron scattering. Therefore in the present work we performed detailed SANS examination of AAO membranes with different pore diameters. It should

also be noted that in case of intercalation of magnetic materials inside the pores, neutron scattering brings us information on the magnetic properties of nanocomposites.

2. Samples

Anodic aluminium oxide membranes formed by a two-step anodization technique or nanoimprint technology are well known to possess a uniform pore structure with a hexagonal arrangement of cylindrical channels. High purity aluminium foil was annealed at 823 K in air in order to remove the mechanical stress and enhance the grain size in the metal. The anodization was carried out in a two-electrode cell. After the first anodization for 24 h the alumina film was selectively etched away. After the second anodization and oxidation for 50–100 h oxide layers with thicknesses between 90 and 180 µm were obtained. Enlargement of the pore diameter was carried out by chemical etching of porous films in 0.3 *M* oxalic acid at 303 K for 2.5, 5 and 7 h. The samples are denoted as AA_0h (as-prepared sample without pore widening), AA_2.5h, AA_5h and AA_7h.

To separate the oxide film from the substrate the remaining aluminium was dissolved. In order to prepare Ni nanowire arrays by an electrodeposition technique a layer of Au film was sputtered onto one side of the AAO template to serve as the working electrode.

Electrochemical experiments were carried out in a three-electrode cell at room temperature. The counter electrode was a Pt wire and the reference electrode a saturated Ag/AgCl electrode connected to the cell *via* a Luggin capillary. The nanocomposites of Ni/AAO were denoted as AA_*t*h_Ni_*l*, where *t* is the pore widening time in 0.3 *M* $(COOH)_2$ at 303 K and *l* is the calculated length of Ni nanowires in micrometres.

Electron microscopy and atomic force microscopy have been widely used to achieve direct imaging of the nickel nanowires in the aluminium oxide matrix. For example, high resolution scanning electron microscopy (HRSEM) reveals a regular hexagonal-type structure of nanopores with periodicity $a_0 \simeq 100$ nm (Fig. 1). But these methods cover only local areas of the sample which may not be representative of the whole nanowire assemblies and do not give any information about the magnetic behaviour of the nanocomposite. Our strategy, therefore, has been to carry out a detailed study of nickel nanowires within mesoporous alumina using a polarized SANS technique.

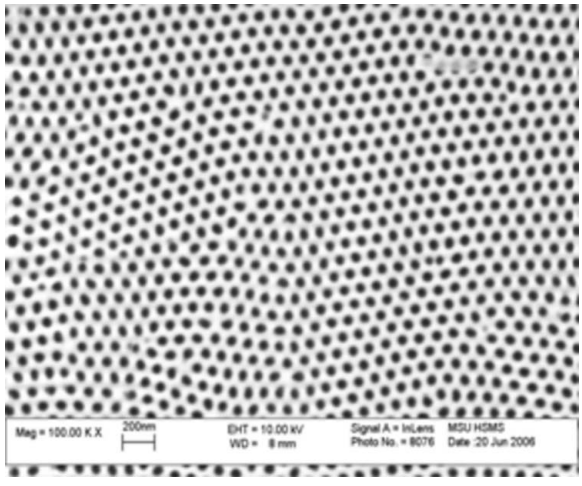

Figure 1
HRSEM data for $AA_{5h}Ni_{100}$, cross-sectional image.

3. Methods

The structure and magnetic properties of the samples described above have been studied by polarized SANS with the SANS-2 instrument at the Geesthacht Neutron Facility (GeNF) in Geesthacht, Germany. A beam of polarized neutrons with initial polarization $P_0 = 0.96$, wavelength $\lambda = 0.58$ nm ($\Delta\lambda/\lambda = 0.1$) and divergence of 1.0 mrad was used. The scattered neutrons were detected with a two-dimensional position-sensitive detector with 256 × 256 pixels. Samples were oriented such that pores were directed parallel to the incident beam (Fig. 2). The magnetic field (0 and 800 mT) was set to be either perpendicular or parallel to the incident beam to reveal the magnetic properties of the system.

A typical scattering pattern for such systems is composed of the diffuse small-angle scattering and the Bragg peak observed as a ring on the detector. This ring is observed instead of a six-spot pattern, which is expected for the hexagonal structure, and corresponds to the scattering on the regular two-dimensional superstructure of nanopores oriented parallel to the incident neutron beam. A large number of defects (see also Fig. 1) leads to a multidomain structure in the sample and results in the isotropic distribution of the scattering intensity in a ring. The diffuse small-angle scattering stems, firstly, from the inhomogeneity of the form of the individual pores/nanowires and, secondly, from the imperfectness of the superstructure itself. Since it is difficult to distinguish between these two sources of the diffuse scattering, we assumed for the sake of simplicity that the two types of scattering (diffuse scattering and small-angle diffraction) are independent. In general, the cross section of polarized neutrons for magnetic samples consists of nuclear (N) and magnetic (M) contributions, as well as a nuclear-magnetic (NM) interference scattering. The scattering intensity for the two polarizations, oriented parallel (+) or antiparallel (−) to the external magnetic field **H**, are given as:

$$I^{\pm}(q) = F_{\rm N}^2(q) + [F_{\rm M}^2(q)\mathbf{m}_{\rm d\perp}^2 \pm 2\langle \mathbf{P}_0\mathbf{m}_{\rm d\perp}\rangle F_{\rm N}(q)F_{\rm M}(q)] + \Phi_{\rm N}^2\Lambda(q-q_{\rm B}) + [\Phi_{\rm M}^2\mathbf{m}_{\rm B\perp}^2 \pm 2\langle \mathbf{P}_0\mathbf{m}_{\rm B\perp}\rangle\Phi_{\rm N}\Phi_{\rm M}]\Lambda(q-q_{\rm B}). \quad (1)$$

Here, q is the modulus of the scattering vector, $q = 4\pi\sin(\theta)/\lambda$, where θ is half the scattering angle, $F_{\rm N}$ and $F_{\rm M}$ are the nuclear and magnetic form factors describing diffuse small-angle scattering, and $\Phi_{\rm N}$ and $\Phi_{\rm M}$ are those describing Bragg reflection, $\Lambda(q)$ is the resolution function of the experimental setup. **m** is the unit vector along the

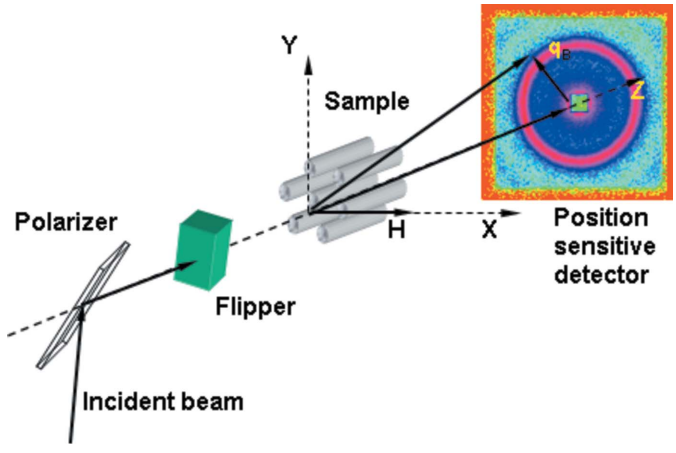

Figure 2
Scheme of the neutron scattering experiment.

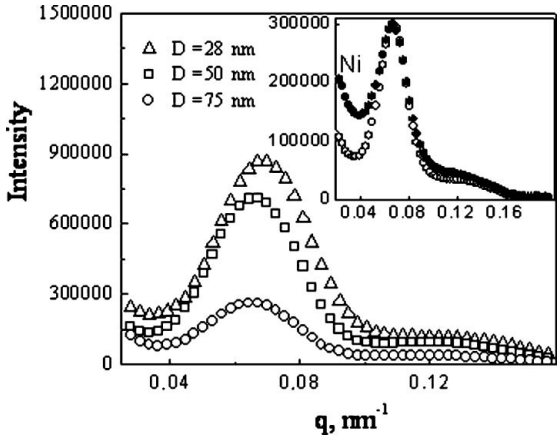

Figure 3
SANS intensity profiles from empty anodic alumina matrices with pore diameters $D \simeq 28$ nm, 50 nm and 75 nm. The inset shows the matrix with $D = 50$ nm: empty one (open symbols), filled with nickel (closed symbols).

magnetization and $\mathbf{m}_\perp = \mathbf{m} - (\mathbf{m}\,\mathbf{e})\mathbf{e}$ with $\mathbf{e} = \mathbf{q}/q$. The subscript symbols d and B refer to the magnetizations attributed to the diffuse scattering and Bragg scattering, respectively. One can assume that $\mathbf{m}_B = \langle \mathbf{m} \rangle$ is the magnetization ascribed to one nanowire but averaged over the whole sample while $\mathbf{m}_d$ is the part of the local magnetization related to the imperfect parts of the nanowires and to a rough approximation $\mathbf{m}_d = \mathbf{m} - \langle \mathbf{m} \rangle$. We determine the total (nuclear and magnetic) scattering as: $I(q) = \frac{1}{2}[I^-(q,\alpha) + I^+(q,\alpha)] = I_N + I_M$. The polarization dependent part of the scattering is determined as the difference $\Delta I(q) = [I^-(q,\alpha) - I^+(q,\alpha)] = I_{NM}$. There are two important features concerning the pure magnetic scattering and the interference scattering. Firstly, the amplitude of the magnetic scattering for Ni is much smaller than that of the nuclear scattering. Therefore, the nuclear scattering is much stronger than the magnetic one. On the other hand, the interference scattering $\Delta I(q)$ is linear with respect to the magnetic form factors, while the pure magnetic scattering contribution to $I(q)$ is quadratic. In this case, the function $\Delta I(q)$ is much more sensitive to the parameters of the magnetic subsystem and we use this fact as an advantage of the polarized neutron scattering compared with the non-polarized one. Secondly, the interference scattering is proportional to $\langle \mathbf{P}_0 \mathbf{m}_\perp \rangle$, *i.e.* to the average magnetization projected onto the external magnetic field, since $\mathbf{P}_0 \parallel \mathbf{H}$. The pure magnetic scattering is proportional to $\langle \mathbf{m}_\perp{}^2 \rangle$, which brings different information in the case where $\mathbf{m}_\perp$ is not collinear to $\mathbf{H}$. This case is of special interest in investigations of strongly anisotropic systems.

4. Results and discussion

The q dependence of the SANS intensity was measured for three different AAO matrices [AA_{0h}, AA_{5h} ($t_{anod} = 100$ h), and AA_{5h} ($t_{anod} = 150$ h) with different treatment and pore diameter ($D \simeq 28$ nm, 50 nm and 75 nm, respectively], in order to characterize a degree of ordering for the pore system. Since the scattering intensity from the matrices was isotropically distributed for both diffuse scattering and Bragg reflection, the data were radially averaged over the whole two-dimensional pattern. The q dependence for these three matrices demonstrates a strong diffraction peak at $q_B \simeq 0.066 \pm 0.002$ nm^{-1} (Fig. 3). Assuming the hexagonal two-dimensional superstructure, the position of this peak corresponds to a period $a_0 \simeq 109 \pm 4$ nm. The intensity of the reflection decreases for the samples which were more intensively treated. This is related to a decreasing amount of the scattering material for the samples with the large pore diameters. Since the width of the peak does not change, the degree of ordering is the same for all three samples. The inset in Fig. 3 shows the SANS patterns for the sample with Ni ($AA_{5h}Ni_{100}$ sample) and that for the empty matrix. We have radially averaged the data for the samples with Ni for the sake of the statistics of the magnetic scattering. Indeed, the magnetic scattering is of the order of a few per cent of the nuclear one and the anisotropic nature of the magnetic contribution has been neglected in this study. The intercalation of nickel into the matrix does not shift the position of the diffraction peak which makes it clear that the matrix was not destroyed by the intercalation. The small-angle scattering ($q < 0.04$ nm^{-1}) increases significantly in samples with Ni. In our opinion, this scattering is caused by the imperfectness of the Ni nanowires inhomogeneously grown within pores (Grigorieva *et al.*, 2005).

The dependence of the magnetic properties of the sample with Ni on the external magnetic field applied perpendicular to the incident beam and to the long axis of the nanowires was studied. The pure magnetic contribution to the scattering, or the field-induced scattering, was extracted as $I_{\mathbf{H}}(q) = I(q,\mathbf{H}) - I(q,0)$. This quantity is shown in Fig. 4 for different values of the magnetic field. It should be noticed that in this treatment not only is the nuclear contribution subtracted but also the magnetic diffuse scattering. Nevertheless the Bragg reflections from the magnetic superstructure are perfectly revealed by this treatment. The intensity of the Bragg reflections increases with the magnetic field. This scattering is attributed to the formation of the magnetic structure composed of the magnetic nanowires.

The scattering intensity was integrated over the Bragg peak and plotted as a function of the magnetic field (Fig. 5). The measurements reveal a large hysteresis in the field dependent part of the cross section $I_{\mathbf{H}}(q)$. This type of behaviour under a magnetic field applied perpendicularly to nanowires is quite typical and was observed in samples with Fe embedded in silicon oxide (Grigorieva *et al.*, 2005). This complex behaviour is caused by interplay of the Zeeman energy (interaction between the magnetic moment and the field) and the large structural anisotropy.

The interference term shows the correlations existing in the system between nuclear and magnetic objects and, as was shown above, it is proportional to the average magnetization of the system. The

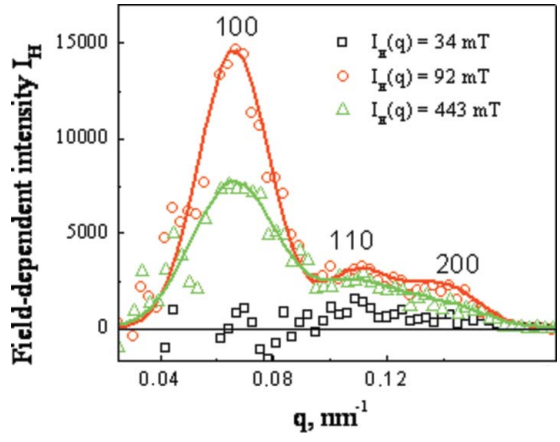

Figure 4
The field-dependent part of the neutron scattering cross section for the sample with Ni at $T = 300$ K and $\mathbf{H} = 34$ mT, 92 mT and 443 mT.

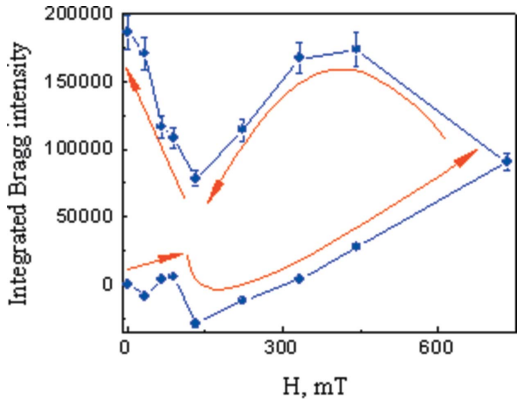

Figure 5
The integrated intensity at the diffraction peak position (**H** ∥ **X**, see Fig. 2) for the sample with Ni.

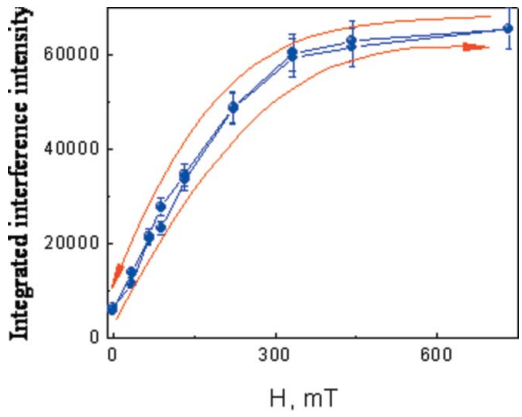

Figure 7
Field dependence of the integrated interference intensity (**H** ∥ **x**, see Fig. 2) at the diffraction peak position for the sample with Ni.

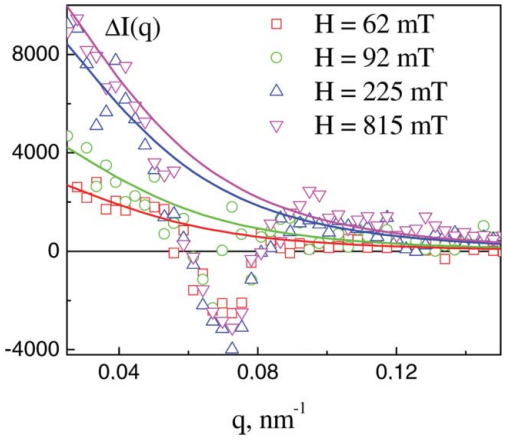

Figure 6
The q dependence of the nuclear-magnetic interference term for the sample with Ni.

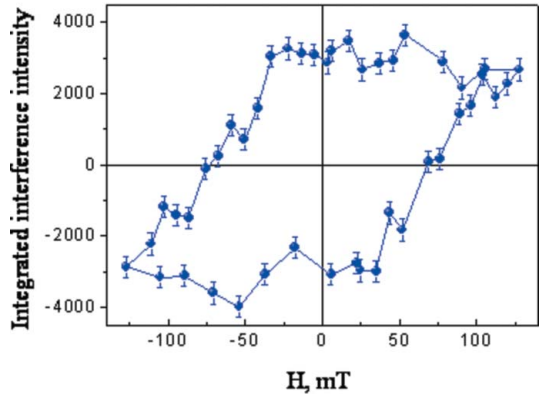

Figure 8
Field dependence of the integrated interference intensity (**H** ∥ **z**, see Fig. 2) at the diffraction peak position for the sample with Ni.

nuclear-magnetic interference $\Delta I(q)$ is observed over the whole q range under study (Fig. 6). The two types of contributions to the interference scattering, the diffuse small-angle scattering and Bragg reflection, appeared to have opposite signs. We fitted the diffuse contribution using the function $I(q) = A(q^2 + R_d^{-2})^{-2}$ where R_d is a characteristic size of the inhomogeneities and A is a constant. The interference contribution to the Bragg peak was obtained by subtracting the experimental points from the extrapolated values.

The integrated interference intensity averaged over the Bragg contribution is shown as a function of the field in Fig. 7. As can be clearly seen this quantity increases linearly with field at $\mathbf{H} < 150$ mT and then tends towards saturation at $\mathbf{H} > 300$ mT. No hysteresis is observed for this interference contribution upon increase and consequent decrease of the magnetic field. The interpolated values of the diffuse interference contribution averaged over the whole q range demonstrates a similar magnetic field dependence but of the opposite sign. It is interesting to compare the magnetic field behaviour of the magnetic cross section $I_{\mathbf{H}}$ (Fig. 5) with that of the interference scattering ΔI (Fig. 7). The interference scattering reflects the behaviour of the average magnetization projected onto the magnetic field applied perpendicularly to the long axis of the nanowires. The magnetic cross section is connected to the autocorrelation function of the magnetization, which reflects the degree of the coherence of the magnetization in different nanowires over the whole sample. The difference between the figures demonstrates that the magnetization process proceeds in a much more complex way than is observed in a simple magnetization measurement using standard methods of magnetometry.

To show the strong magnetic anisotropy of the sample, we applied the external magnetic field parallel to the long axis of the nanowires. It is worth noting that no change for the pure magnetic contribution $I_{\mathbf{H}}(q)$ was detected within the error bars, while the interference term changed significantly. The interference scattering is composed again of the two types of contributions of opposite signs, similar to the case shown in Fig. 6. The integrated interference intensity averaged over the Bragg contribution is shown as a function of the field in Fig. 8. A large hysteresis is observed upon increase and consequent decrease of the magnetic field with the coercive field equal to 75 ± 3 mT. The magnetic system is fully magnetized at $\mathbf{H} \sim 100$ mT and it stays frozen upon decrease of the field up to the negative values of 35 ± 3 mT. Again the magnetic behaviour of the magnetic cross section I_H is different from that of the interference scattering. A comparison of Figs. 7 and 8 shows that there is a big difference in the magnetization process of the sample for the field applied parallel to the long axis of nanowires or perpendicular to it. The additional details of the magnetization process may be extracted from the behaviour of the pure magnetic contribution to the scattering.

5. Conclusions

In conclusion, the study demonstrates the possibilities of polarized SANS for investigating the structure and magnetic properties of two-dimensional spatially ordered systems of ferromagnetic nanowires. The importance of the study is related to the fact that this system is a promising candidate for high-density data storage devices.

The authors thank the administration of GKSS for kind hospitality, Ministry of Science and Education RF (goscontract 02.434.11.2022) and RFBR (projects 04-02-17509, 07-02-01151).

References

Benfield, R. E., Grandjean, D., Dore, J. C., Esfahanian, H., Wu, Z., Kröll, M., Geerkens, M. & Schmid, G. (2004). *Faraday Discuss.* **125**, 327–342.
Grigorieva, N. A., Grigoriev, S. V., Okorokov, A. I., Eckerlebe, H., Eliseev, A. A., Lukashin, A. V. & Napolskii, K. S. (2005). *Physica E*, **28**, 286–295.
Jessensky, O., Müller, F. & Gösele, U. (1998). *J. Electrochem. Soc.* **145**, 3735–3740.
Li, F., Zhang, L. & Metzger, R. M. (1998). *Chem. Mater.* **10**, 2470–2480.
Masuda, H., Hasegwa, F. & Ono, S. (1997). *J. Electrochem. Soc.* **144**, L127–L130.
Nielsch, K., Choi, J., Schwirn, K., Wehrspohn, R. B. & Gösele, U. (2002). *Nano Lett.* **2**, 677–680.